Pressure-based vortex extraction in cardiac 4D PC-MRI blood flow data

B. Köhler[1], M. Grothoff[2], M. Gutberlet[2], and B. Preim[1]

[1]Dept. of Computer Graphics and Simulation, Magdeburg University, Germany
[2]Dept. of Diagnostic and Interventional Radiology, Heart Center Leipzig, Germany

Abstract

We propose a technique for vortex extraction in cardiac 4D PC-MRI blood flow data that employs an intravascular, relative pressure calculation. The method is easy to implement, runs fully automatically, and requires no user-defined parameters. We qualitatively evaluated 100+ *datasets of the aorta, pulmonary artery, or left ventricle from healthy volunteers as well as from patients acquired with different MR scanners. In all cases, the results suffer from significantly less noise than comparable approaches using the common* λ_2 *vortex criterion.*

Categories and Subject Descriptors (according to ACM CCS): I.4.9 [Computing Methodologies]: Image Processing and Computer Vision—Applications J.3 [Computer Applications]: Life and Medical Sciences—

1. Introduction

Four-dimensional phase-contrast magnetic resonance imaging [WSW96] (4D PC-MRI) facilitates the assessment of 3D blood flow velocity vectors of one heart beat. Common flow visualization techniques, such as pathlines, enable a qualitative analysis of occurring flow patterns. Vortex flow was linked to various cardiovascular diseases, e.g., aneurysm development in patients with bicuspid aortic valves [BHB*13] and in patients with narrowed vessel sections [FAH*08]. Some methods to extract such flow features employ assumptions about the flow's local pressure characteristics. For 4D PC-MRI data, there is a group of specialized techniques to calculate relative, intravascular pressure [KBV*17]. To the best of our knowledge, no one yet used the latter group of methods for the purpose of vortex flow extraction. In this work, we show that this approach is superior to conventional techniques.

2. Related Work

Vortex flow extraction: Vortex extraction methods either yield vortex core lines or vortex regions. Günther and Theisel [GT18] summarized the state of the art. *Local* techniques usually operate on the velocity vectors and their derivatives. Typical measures are vorticity, helicity, the Q criterion, reduced velocity, and torsion. The λ_2 criterion [JH95] assumes that there are local pressure minima inside a vortex. From the Navier-Stokes, the vorticity transport and the strain-rate transport equations, a calculation based on the vector field's Jacobian matrix J is derived: $\{\lambda_1 \geq \lambda_2 \geq \lambda_3\} = \mathrm{eig}(S^2 + \Omega^2)$ with $S = 1/2 \cdot (J + J^T)$ and $\Omega = 1/2 \cdot (J - J^T)$ A vortex exists where the second eigenvalue is negative ($\lambda_2 < 0$). *Global* techniques incorporate more of the domain and, thus, are computationally more expensive. They are, for instance, based on the integral lines' winding angles.

4D PC-MRI: Surveys about 4D PC-MRI were published by Dyverfeldt et al. [DBB*15] in a consensus statement and by Nayak et al. [NNB*15]. Köhler et al. [KBV*17] provided an overview about the data processing pipeline from a technical perspective.

Vortex flow extraction in 4D PC-MRI data: Vortex extraction in 4D PC-MRI data is challenging due to low spatio-temporal image resolution, noise, magnetic field-related MR artifacts, and motion-related artifacts due to vascular pulsation and breathing. Köhler et al. [KGP*13] compared the results of different local vortex criteria for the cardiac context. They found λ_2 as most suitable and proposed a semi-automatic, three-step procedure to extract high-quality, vortex flow-representing pathlines using line predicate-based filtering [SS06, BPM*13]. They first calculated the λ_2 criterion for each pathline point, then smoothed the values along each pathline with a binomial filter. Subsequently, average λ_2 values for connected pathline sections were determined where λ_2 is constantly above a given threshold. In a last post-processing step, short and straight lines were filtered out using a bending energy predicate. Elbaz et al. [ECW*14] used the λ_2 criterion to extract left ventricular vortex rings – a mechanism to optimize blood transport. Other approaches employed cross-sectional vector pattern matching [HEWK03, VFCV14] to find swirling flow structures.

Relative pressure in 4D PC-MRI data: Relative pressure is an important measure to assess the degree of vessel narrowings (stenosis). Pressure drops are a typical observation, i.e., high and low pressure before and behind the narrowing, respectively.

Tyszka et al. [TLAS00] described an iterative solver for the pressure Poisson equation (PPE), which is based on the Navier-Stokes equations, to obtain relative pressure inside the vessel. This was the basis for more refined methods that separated pressure into transient, convective, and viscous components [LPK*14], or methods that used the work-energy equation instead of PPE [DFS*15], or methods that used geometric models instead of segmentations to describe the vessel lumen [MRG*14]. Schumann and Hennemuth [SH15] presented a custom minimum / maximum intensity projection to visualize pressure maps via volume rendering. They also provided diagrams of the average, relative pressure along a centerline to evaluate pressure drops.

3. Data Acquisition and Pre-Preprocessing

Our data were acquired with at least five different 4D PC-MRI sequences using 1.5 [T] and 3 [T] MR scanners from Siemens and Philips. Typical spatio-temporal resolutions are about 1.5–2 × 1.5–2 × 2–3 [mm]/40–60 [ms] in a $140 \times 200 \times 25/20$ grid.

A 3D segmentation, as approximation of the dynamic vessel, is carried out using a graph cut [BK04]. A surface is subsequently extracted via marching cubes and smoothed.

We integrate 30,000 pathlines via RK4. The seeds are uniformly distributed over time within the vessel segmentation. Our employed line visualization enhances aberrant flow patterns [KGGP17].

4. Methods

In the sense of the λ_2 criterion, we employ relative pressure as an indicator of vortex regions. But instead of a purely local computation, we use the iterative approach for the whole vessel by Tyszka et al. [TLAS00]. The implementation is detailed in Algorithm 1. The values for viscosity and density are derived from related literature [PS05, BFL*11].

The original method stops on convergence. We use a fixed number of 1,000 iterations instead. This allows us to more easily and accurately provide a progress bar during computation for a better user experience. For each of our datasets, the calculation converges below 1,000 iterations, so we assume this upper threshold as safe.

We smooth each temporal position of the resulting 4D, scalar, relative pressure map separately with a $3 \times 3 \times 3$ binomial filter (1 iteration). Then, we clamp the values to the 1 % and 99 % quantile to increase robustness against outliers. Afterwards, we re-shift the values so that they are relative to the average again, i.e., the mean of all time steps is subtracted from each value. We convert the values from [Pa] to [mmHg], since this is commonly used in the cardiac context and preferred by our clinical collaborators. All of these steps are applied only within the binary vessel segmentation.

Analogous to vortex regions defined as $\lambda_2 < 0$, a relative pressure $P < 0$ [mmHg] is required. We employ line predicate-based filtering to extract the pathline parts within vortex regions. I.e., P is interpolated linearly from the pressure map for each pathline point, and a pathline segment consisting of two subsequent points is only shown if the average P of these points is below the threshold.

Algorithm 1 Relative pressure calculation [TLAS00].

function CALC_RELATIVE_PRESSURE(F [$\mathbb{R}^4 \to \mathbb{R}^3$ flow field])
  Density = 1,060.0 [kg/m^3]
  Viscosity = 0.0035 [Pa·s]
  $\vec{gs}$ = F.size() [4D grid size]
  $\vec{sc}$ = F.scale() [4D spatio-temporal resolution]
  P = $\vec{0}$ [4D scalar image of size $\vec{gs}$]
  for v = 0 **to** num vessels − 1 **do** [for each vessel separately]
    S = 3D binary vessel segmentation
    [***** GENERATE PRESSURE GRADIENT *****]
    ∇P = $\vec{0}$ [4D vec3 image of size $\vec{gs}$]
    for $\begin{bmatrix} x \\ y \\ z \end{bmatrix} = \begin{bmatrix} 0 \\ 0 \\ 0 \end{bmatrix}$ **to** $\begin{bmatrix} \vec{gs}[0]-1 \\ \vec{gs}[1]-1 \\ \vec{gs}[2]-1 \end{bmatrix}$ **do**
      if $S_{x,y,z} == 0$ **then continue** [outside vessel]
      for $t = 0$ **to** $\vec{gs}[3]-1$ **do** [Eq. 1 in [TLAS00]]
        $\mathrm{dvdt} = \left(F^{t+1}_{x,y,z} - F^{t-1}_{x,y,z}\right) \Big/ \left(2 \cdot \vec{sc}[3]\right)$ [vec3]
        lapV = $\vec{0}$ [vec3]
        for $i = 0$ **to** 2 **do**
          $\mathrm{lapV}[i] = F^{t}_{x-1,y,z} + F^{t}_{x+1,y,z} - 2 \cdot F^{t}_{x,y,z} / \vec{sc}[0]^2$
          $\mathrm{lapV}[i] = F^{t}_{x,y-1,z} + F^{t}_{x,y+1,z} - 2 \cdot F^{t}_{x,y,z} / \vec{sc}[1]^2$
          $\mathrm{lapV}[i] = F^{t}_{x,y,z-1} + F^{t}_{x,y,z+1} - 2 \cdot F^{t}_{x,y,z} / \vec{sc}[2]^2$
        $\mathrm{dx} = \left(F^{t}_{x+1,y,z} - F^{t}_{x-1,y,z}\right) \Big/ \left(2 \cdot \vec{sc}[0]\right)$ [vec3]
        $\mathrm{dy} = \left(F^{t}_{x,y+1,z} - F^{t}_{x,y-1,z}\right) \Big/ \left(2 \cdot \vec{sc}[1]\right)$ [vec3]
        $\mathrm{dz} = \left(F^{t}_{x,y,z+1} - F^{t}_{x,y,z-1}\right) \Big/ \left(2 \cdot \vec{sc}[2]\right)$ [vec3]
        vdv = $\vec{0}$ [vec3]
        for $i = 0$ **to** 2 **do** $\mathrm{vdv}[i] = \mathrm{dot}\left(F^{t}_{x,y,z}, \begin{bmatrix} \mathrm{dx}[i] \\ \mathrm{dy}[i] \\ \mathrm{dz}[i] \end{bmatrix}\right)$
        $\nabla P^{t}_{x,y,z} = (\mathrm{dvdt} + \mathrm{vdv}) \cdot \mathrm{Density} - \mathrm{lapV} \cdot \mathrm{Viscosity}$
    [***** CALCULATE RELATIVE PRESSURE *****]
    Pk[2] = {0, 0} [2 4D scalar images of size $\vec{gs}$]
    for $i = 0$ **to** 999 **do** [1,000 iterations]
      $r = \mathrm{Pk}[\mathrm{mod}(i, 2)]$ [alternating read/write]
      $w = \mathrm{Pk}[\mathrm{mod}(i+1, 2)]$
      for $\begin{bmatrix} x \\ y \\ z \end{bmatrix} = \begin{bmatrix} 0 \\ 0 \\ 0 \end{bmatrix}$ **to** $\begin{bmatrix} \vec{gs}[0]-1 \\ \vec{gs}[1]-1 \\ \vec{gs}[2]-1 \end{bmatrix}$ **do**
        if $S_{x,y,z} == 0$ **then continue** [outside vessel]
        for $t = 0$ **to** $\vec{gs}[3]-1$ **do** [Eq. 5 in [TLAS00]]
          $w^{t}_{x,y,z} = r^{t}_{x,y,z} \;/\; 2$ [with $\alpha = 0.5$]
          $w^{t}_{x,y,z} \overset{+}{=} \left(r^{t}_{x-1,y,z} + r^{t}_{x+1,y,z}\right) / 12$
          $w^{t}_{x,y,z} \overset{+}{=} \left(r^{t}_{x,y-1,z} + r^{t}_{x,y+1,z}\right) / 12$
          $w^{t}_{x,y,z} \overset{+}{=} \left(r^{t}_{x,y,z-1} + r^{t}_{x,y,z+1}\right) / 12$
          $w^{t}_{x,y,z} \overset{+}{=} \vec{sc}[0] \cdot \left(\nabla P^{t}_{x+1,y,z} - \nabla P^{t}_{x-1,y,z}\right) / 12$
          $w^{t}_{x,y,z} \overset{+}{=} \vec{sc}[1] \cdot \left(\nabla P^{t}_{x,y+1,z} - \nabla P^{t}_{x,y-1,z}\right) / 12$
          $w^{t}_{x,y,z} \overset{+}{=} \vec{sc}[2] \cdot \left(\nabla P^{t}_{x,y,z+1} - \nabla P^{t}_{x,y,z-1}\right) / 12$
    copy last w to P if inside S
  return P

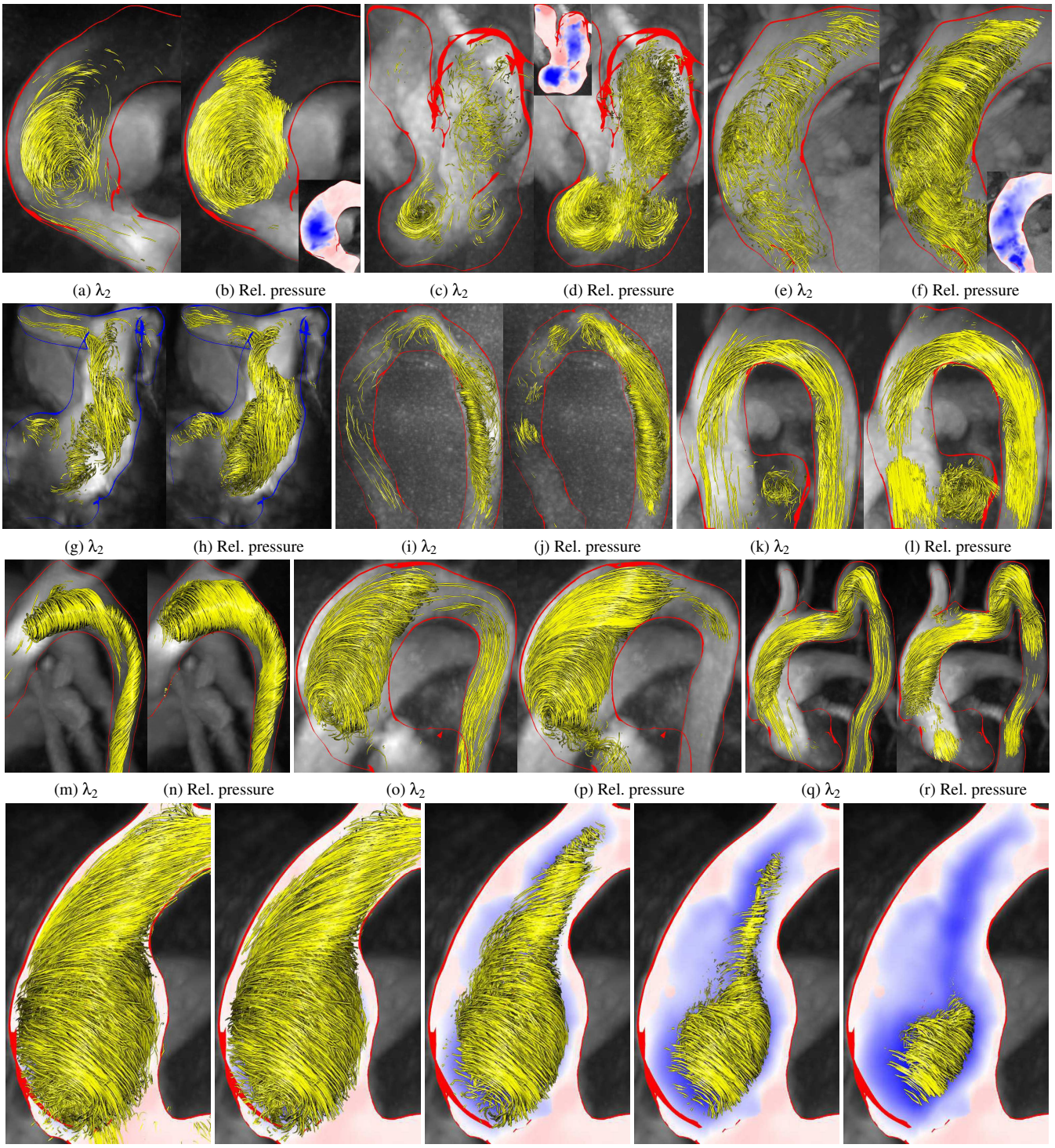

(a) λ_2 (b) Rel. pressure (c) λ_2 (d) Rel. pressure (e) λ_2 (f) Rel. pressure

(g) λ_2 (h) Rel. pressure (i) λ_2 (j) Rel. pressure (k) λ_2 (l) Rel. pressure

(m) λ_2 (n) Rel. pressure (o) λ_2 (p) Rel. pressure (q) λ_2 (r) Rel. pressure

(s) $P < +0.5$ [mmHg] (t) $P < 0$ [mmHg] (u) $P < -2$ [mmHg] (v) $P < -4$ [mmHg] (w) $P < -6$ [mmHg]

Figure 1: Results of a healthy volunteer (k–l), or patients with aneurysms (a–b, o–p, s–w), aortic valve defects (e–f, m–n), an aortic arch prosthesis (i–j), an aortic arch bypass (q–r), an insufficient pulmonary valve (g–h), or with a mitral valve defect (c–d). Except for the bottom row, side by side comparisons between extracted pathlines using the λ_2 criterion and relative pressure are shown. The bottom row shows relative pressure-based filtering with increasingly strict thresholding. The top and bottom rows additionally show pressure maps at the corresponding temporal positions. Red and blue corresponds to relative pressure above and below intravascular average, respectively.

5. Results and Discussion

Fig. 1 shows ten diverse datasets. The top and bottom rows additionally show the pressure maps at the corresponding temporal positions. Figs. k–l show the systolic blood flow of a healthy volunteer. There is a slight helix in the aortic arch, which is normal behavior. Figs. a–b, o–p, and s–w show aneurysm patients during systole. All have severe vortex flow in the widened ascending aorta. A similar behavior can be observed in aortic valve defect patients (Figs. e–f and m–n). Prominent vortex flow emerges in the descending aorta of the patient with an aortic arch prosthesis (Figs. i–j). The flow of the patient with an aortic arch bypass (Figs. q–r) forms an elongated helix along the whole ascending aorta and aortic arch. Figs. c–d show the left ventricle and left atrium of a mitral valve defect patient during diastole, when the ventricle is refilled with oxygenated blood. Notice the vortex rings [ECW*14] in the bottom of the images. The pulmonary artery (Figs. g–h) is of a patient with insufficient pulmonary valve. It does not close properly, causing about 30 % retrograde blood flow back into the right ventricle during diastole.

The last row (Figs. s–w) shows pressure-based vortex extraction with different relative pressure thresholds. Stricter thresholds only preserve lines closer to the vortex core. This value can be adapted by the user in real-time if desired.

Performance: The pressure map calculation depends on the size of the vessel segmentation. It did not take longer than 10 s for any of our datasets using an Intel i7-3930K (6×3.2 GHz).

Discussion: Pressure-based vortex extraction revealed the same vortices that were found with the λ_2-based approach. This is plausible, since λ_2 is also motivated by local pressure minima. Moreover, both approaches share the same threshold ($x < 0$) to specify vortex regions. The quality of the extracted pathlines using relative pressure is in many cases superior to λ_2-based filtering, but at least on par with it in all cases. The line bundles often have a higher density.

In healthy volunteers with only insignificant vortex flow, there are many regions within the vessel with a relative pressure smaller than zero. This may result in an increased amount of false positives, i.e., laminar flow lines that are still visible after vortex filtering. This can be alleviated by using, e.g., -0.25 [mmHg] as default threshold for the relative pressure instead of 0 [mmHg]. However, for our clinical collaborators it is more important that smaller vortices are not accidentally removed. Alternatively, a soft threshold could be applied using linear transparency fading so that, e.g., values $P \leq -0.25$ [mmHg] are fully opaque ($\alpha = 1$) and values $P \geq 0$ [mmHg] are fully transparent ($\alpha = 0$).

The post-processing of the pressure map influences the resulting lines. A higher and lower degree of smoothing leads to wider and narrower vortices, respectively. Performing one iteration of binomial smoothing worked best for our database.

Our results (Figs. g–h) are in accordance with medical findings. For instance, Reiter et al. [RRK*15] assessed the disease severity in patients with pulmonary hypertension by inspecting right-ventricular vortex flow.

6. Conclusion and Future Work

We have shown that using specialized methods to calculate relative pressure in 4D PC-MRI data [TLAS00] for vortex extraction is more efficient than conventional approaches [KGP*13]. Relative pressure calculation is easy to implement, especially with the pseudocode provided in this paper. The pressure map calculation is required only once as a pre-processing step.

In the future, the 4D relative pressure map could be used to create flow statistics, e.g., time-dependent percentages of vortical flow for each segmented vessel.

Acknowledgments

This work was funded by the German Research Foundation (PR 660/18-1). We would like to thank Katharina Vellguth and Leonid Goubergrits for providing the mitral valve patient dataset, which is courtesy of the Institute for Imaging Science and Computational Modelling in Cardiovascular Medicine, Charité – Universitätsmedizin Berlin.

References

[BFL*11] Bock J., Frydrychowicz A., Lorenz R., Hirtler D., Barker A. J., Johnson K. M., Arnold R., Burkhardt H., Hennig J., Markl M.: In vivo noninvasive 4D pressure difference mapping in the human aorta: Phantom comparison and application in healthy volunteers and patients. *Journal of Magnetic Resonance Imaging 66*, 4 (2011), 1079–88. doi:10.1002/mrm.22907. 2

[BHB*13] Bissell M. M., Hess A. T., Biasiolli L., Glaze S. J., Loudon M., Pitcher A., Davis A., Prendergast B., Markl M., Barker A. J., Neubauer S., Myerson S. G.: Aortic dilation in bicuspid aortic valve disease: Flow pattern is a major contributor and differs with valve fusion type. *Circulation: Cardiovascular Imaging 6*, 4 (2013), 499–507. doi:10.1161/CIRCIMAGING.113.000528. 1

[BK04] Boykov Y., Kolmogorov V.: An experimental comparison of min-cut / max-flow algorithms for energy minimization in vision. *IEEE Transactions on Pattern Analysis and Machine Intelligence 26*, 9 (2004), 1124–37. doi:10.1109/TPAMI.2004.60. 2

[BPM*13] Born S., Pfeifle M., Markl M., Gutberlet M., Scheuermann G.: Visual analysis of cardiac 4D MRI blood flow using line predicates. *IEEE Transactions on Visualization and Computer Graphics 19* (2013), 900–12. doi:10.1109/TVCG.2012.318. 1

[DBB*15] Dyverfeldt P., Bissell M., Barker A. J., Bolger A. F., Carlhäll C.-J., Ebbers T., François C. J., Frydrychowicz A., Geiger J., Giese D., Hope M. D., Kilner P. J., Kozerke S., Myerson S., Neubauer S., Wieben O., Markl M.: 4D flow cardiovascular magnetic resonance consensus statement. *Journal of Cardiovascular Magnetic Resonance 17*, 1 (2015), 1–19. doi:10.1186/s12968-015-0174-5. 1

[DFS*15] Donati F., Figueroa C. A., Smith N. P., Lamata P., Nordsletten D. A.: Non-invasive pressure difference estimation from PC-MRI using the work-energy equation. *Medical Image Analysis 26*, 1 (2015), 159–72. doi:10.1016/j.media.2015.08.012. 2

[ECW*14] Elbaz M. S. M., Calkoen E. E., Westenberg J. J. M., Lelieveldt B. P. F., Roest A. A. W., Van der Geest R. J.: Vortex flow during early and late left ventricular filling in normal subjects: Quantitative characterization using retrospectively-gated 4D flow cardiovascular magnetic resonance and three-dimensional vortex core analysis. *Journal of Cardiovascular Magnetic Resonance 16*, 78 (2014), 12. doi:10.1186/s12968-014-0078-9. 1, 4

[FAH*08] Frydrychowicz A., Arnold R., Hirtler D., Schlensak C., Stalder A. F., Hennig J., Langer M.,

MARKL M.: Multidirectional flow analysis by cardiovascular magnetic resonance in aneurysm development following repair of aortic coarctation. *Journal of Cardiovascular Magnetic Resonance 10*, 30 (2008). doi:10.1186/1532-429X-10-30. 1

[GT18] GÜNTHER T., THEISEL H.: The state of the art in vortex extraction. *CGF* (2018), in print. doi:10.1111/cgf.13319. 1

[HEWK03] HEIBERG E., EBBERS T., WIGSTRÖM L., KARLSSON M.: Three-dimensional flow characterization using vector pattern matching. *IEEE Transactions on Visualization and Computer Graphics 9*, 3 (2003), 313–9. doi:10.1109/TVCG.2003.1207439. 1

[JH95] JEONG J., HUSSAIN F.: On the identification of a vortex. *Journal of Fluid Mechanics 285* (1995), 69–94. doi:10.1017/S0022112095000462. 1

[KBV*17] KÖHLER B., BORN S., VAN PELT R. F. P., HENNEMUTH A., PREIM U., PREIM B.: A survey of cardiac 4D PC-MRI data processing. *Computer Graphics Forum 36*, 6 (2017), 5–35. doi:10.1111/cgf.12803. 1

[KGGP17] KÖHLER B., GROTHOFF M., GUTBERLET M., PREIM B.: Visualization of cardiac blood flow using anisotropic ambient occlusion for lines. In *Proc: Vision, Modelling und Visualization (VMV)* (2017). 2

[KGP*13] KÖHLER B., GASTEIGER R., PREIM U., THEISEL H., GUTBERLET M., PREIM B.: Semi-automatic vortex extraction in 4D PC-MRI cardiac blood flow data using line predicates. *IEEE Transactions on Visualization and Computer Graphics 19*, 12 (2013), 2773–82. doi:10.1109/TVCG.2013.189. 1, 4

[LPK*14] LAMATA P., PITCHER A., KRITTIAN S. B. S., NORDSLETTEN D., BISSELL M. M., CASSAR T., BARKER A. J., MARKL M., NEUBAUER S., SMITH N. P.: Aortic relative pressure components derived from four-dimensional flow cardiovascular magnetic resonance. *Journal of Magnetic Resonance Imaging 72*, 4 (2014), 1162–9. doi:10.1002/mrm.25015. 2

[MRG*14] MIHALEF V., RAPAKA S., GÜLSÜN M. A., SCORZA A., SHARMA P., ITU L. M., KAMEN A., BARKER A. J., MARKL M., COMANICIU D.: Model-based estimation of 4D relative pressure map from 4D flow MR images. In *Proceedings: Statistical Atlases and Computational Models of the Heart. Imaging and Modelling Challenges (STACOM)* (2014), pp. 236–43. doi:10.1007/978-3-642-54268-8_28. 2

[NNB*15] NAYAK K. S., NIELSEN J.-F., BERNSTEIN M. A., MARKL M., GATEHOUSE P. D., BOTNAR R. M., SALONER D., LORENZ C., WEN H., HU B. S., EPSTEIN F. H., OSHINSKI J. N., RAMAN S. V.: Cardiovascular magnetic resonance phase contrast imaging. *Journal of Cardiovascular Magnetic Resonance 17*, 71 (2015), 1–26. doi:10.1186/s12968-015-0172-7. 1

[PS05] PAPAIOANNOU T. G., STEFANADIS C.: Vascular wall shear stress: Basic principles and methods. *Hellenic Journal of Cardiology 46*, 1 (2005), 9–15. 2

[RRK*15] REITER G., REITER U., KOVACS G., OLSCHEWSKI H., FUCHSJÄGER M.: Blood flow vortices along the main pulmonary artery measured with MR imaging for diagnosis of pulmonary hypertension. *Radiology 275*, 2 (2015), 71–9. doi:10.1148/radiol.14140849. 4

[SH15] SCHUMANN C., HENNEMUTH A.: Three-dimensional visualization of relative pressure in vascular structures. In *Proceedings: Computer and Robot Assisted Surgery (CURAC)* (2015), pp. 337–41. 2

[SS06] SALZBRUNN T., SCHEUERMANN G.: Streamline predicates. *IEEE Transactions on Visualization and Computer Graphics 12*, 6 (2006), 1601–12. doi:10.1109/TVCG.2006.104. 1

[TLAS00] TYSZKA J. M., LAIDLAW D. H., ASA J. W., SILVERMAN J. M.: Three-dimensional, time-resolved (4D) relative pressure mapping using magnetic resonance imaging. *Journal of Magnetic Resonance Imaging 12*, 2 (2000), 321–9. doi:10.1002/1522-2586(200008)12:2<321::AID-JMRI15>3.0.CO;2-2. 2, 4

[VFCV14] VAN PELT R. F. P., FUSTER A., CLAASSEN G. G. H., VILANOVA A.: Characterization of blood-flow patterns from phase-contrast MRI velocity fields. In *Eurographics Conference on Visualization (EuroVis) - Short Papers* (2014). doi:10.2312/eurovisshort.20141158. 1

[WSW96] WIGSTRÖM L., SJÖQVIST L., WRANNE B.: Temporally resolved 3D phase-contrast imaging. *Journal of Magnetic Resonance Imaging 36*, 5 (1996), 800–3. doi:10.1002/mrm.1910360521. 1